Chapter 19

Enantiospecific Properties of Chiral Single-Crystal Surfaces

Joshua D. Horvath, Andrew J. Gellman*, David S. Sholl, and Timothy D. Power

Department of Chemical Engineering, Carnegie Mellon University, Pittsburgh, PA 15213

Single crystalline surfaces with structures having kinked steps are inherently chiral. As such these surfaces have enantiospecific properties that have been explored both theoretically and experimentally. Experimental studies of adsorption have been performed using two chiral adsorbates ((S)-1-chloro-2-methylbutane and (R)-3-methylcyclohexanone) on chiral $Cu(643)^R$ and $Cu(643)^S$ surfaces. Preliminary work has shown desorption kinetics for (R)-3-methylcyclohexanone adsorption that are influenced by the handedness of the Cu(643) surface. Theoretical simulation of the adsorption of small chiral molecules on chiral Pt surfaces has been used to attempt to understand the role of surface and adsorbate characteristics in determining enantiospecificity.

Introduction

A type of chiral surface is generated when crystalline surfaces are terminated in structures with kinked steps. McFadden *et al.* first described kinked chiral surfaces such as the (643) and $(\overline{643})$ surfaces of a face-centered cubic crystal (fcc) that are nonsuperimposable mirror images of each other. They proposed a naming convention for chiral surfaces that is analogous to the Cahn-Ingold-Prelog rules for naming chiral organic molecules.[1] The (643)

surface was designated $(643)^S$ and the $(\overline{643})$ surface was designated $(643)^R$. To determine if enantiospecific adsorption of molecules on chiral single crystal surfaces could be observed, McFadden *et al.* examined the adsorption of (R)- and (S)-butan-2-ol on $Ag(643)^R$ and $Ag(643)^S$ surfaces.[1] Two experiments designed to detect enantiospecific interactions between the chiral Ag(643) surfaces and these chiral alcohols were conducted. The first experiment measured the desorption energies of (R)- and (S)-butan-2-ol from the $Ag(643)^R$ and $Ag(643)^S$ surfaces. The second experiment measured the activation barriers to β-hydride elimination for (R)- and (S)-butan-2-oxide on the $Ag(643)^R$ and $Ag(643)^S$ surfaces. No enantiospecific energy differences greater than ~0.1 kcal/mol were found for either of these systems. If the adsorption of these molecules was influenced by the chirality of the surface, the differences were too small to measure.

A later theoretical paper by Sholl describes the adsorption of chiral hydrocarbons on the chiral Pt(643) surface.[2] Binding energies of several chiral hydrocarbons adsorbed on Pt(643) were calculated using Monte Carlo simulations. The chiral molecules limonene, 1,2-dimethylcyclopropane, and 1,2-dimethylcyclobutane have predicted binding energies that differ significantly between the two enantiomers of the same chiral compound. These theoretical results suggest that for several chiral hydrocarbons on Pt(643), the enantiospecific desorption energy differences are large enough to measure experimentally.

More recently, experiments by Attard *et al.* investigated the electro-oxidation of the chiral molecule glucose at chiral platinum electrodes.[3,4] They also proposed a more general nomenclature for the chirality of high Miller index fcc surfaces based on the orientations of the planes that form the steps and kinks. As expected, the *achiral* Pt(211) and Pt(332) electrodes did not demonstrate enantiospecific differences between the rates of oxidation of D- and L-glucose. On the other hand, the *chiral* Pt(643) and Pt(531) electrodes did show enantiospecific oxidation of the two enantiomers of glucose. This was the first experimental demonstration of the enantiospecific adsorption properties of chiral single-crystal surfaces.

To determine if enantiospecific adsorption of chiral organic molecules can be detected on the $Cu(643)^R$ and $Cu(643)^S$ surfaces, we have investigated the desorption of (S)-1-chloro-2-methylbutane and (R)-3-methylcyclohexanone from the chiral Cu(643) surfaces using temperature programmed desorption (TPD).

Experimental Section

All experiments were conducted in a stainless steel chamber built to achieve ultrahigh vacuum conditions. A titanium sublimation pump and a cryopump produce a base pressure of less than 10^{-10} Torr. The chamber is equipped with a quadrupole mass spectrometer, used to perform TPD and other analyses of the gas composition in the chamber. Two leak valves are installed to introduce gases and vapors into the chamber. One leak valve has a ½ inch diameter dosing tube terminating two inches from the center of the chamber. This allows the crystal to be positioned directly in front of the vapor stream flowing into the chamber through the leak valve. The other leak valve does not have a dosing tube and is used for background (non-line-of-sight) exposures. Exposures are reported in Langmuirs (1 L = 1.0 x 10^{-6} Torr-sec) and are not corrected for ion gauge sensitivity to different gas species. A sputter ion gun is installed to perform inert gas ion etching (cleaning) of surfaces. A four-grid retarding field analyzer is used to perform low energy electron diffraction (LEED) experiments and Auger electron spectroscopy (AES).

A single crystal Cu disk 12.5 mm in diameter and 2 mm thick was purchased from Monocrystals Company. One side of the sample exposes the (643) surface, and the other side of the sample exposes the $(\overline{6}\overline{4}\overline{3})$ surface. The crystal was spot-welded between two tantalum wires attached to a sample holder, at the bottom of a manipulator. The manipulator allows 360-degree rotation of the crystal about the chamber axis and movement in the x, y, and z directions. The crystal could be cooled with liquid nitrogen to less than 90 K and heated resistively to over 1000 K. The crystal temperature is measured by a chromel/alumel thermocouple junction spot-welded to the top edge of the crystal. During heating the sample temperature is computer controlled to ensure a linear heating profile.

Both sides of the crystal were initially cleaned by cycles of 1.0 keV argon ion bombardment and annealing to 950 K until no contaminants were detected by AES. Each of the chiral adsorbates investigated in this paper were found to contaminate the surface with carbon after cumulative exposures greater than 1 L. To remove carbon contamination after each experiment, the surface was cleaned by several 15-minute cycles of 1.0 keV argon ion sputtering and annealing to 950K. The surface cleanliness was verified by AES and the (643) structure was verified by sharp LEED patterns.

The chiral adsorbates we have used are liquid at room temperature and have relatively high vapor pressures, allowing them to be introduced to the vacuum chamber through leak valves. (S)-1-chloro-2-methylbutane and a racemic mixture of (R/S)-1-chloro-2-methylbutane were obtained from TCI American at 99% purity. (R)-3-methylcyclohexanone (99%) and a racemic mixture of (R/S)-3-methylcyclohexanone (97%) were obtained from Aldrich Chemical. The

chiral compounds were each transferred to glass vials and subjected to several cycles of freezing, pumping, and thawing to remove dissolved air or other high pressure impurities. The purity of each sample was verified by mass spectrometry.

Temperature programmed desorption experiments were performed by cooling the Cu(643) surface with liquid nitrogen to less than 90 K. The clean Cu(643) surface was then exposed to vapors admitted to the chamber through a leak valve. Exposures of (S)-1-chloro-2-methylbutane and its racemic mixture were performed with the Cu crystal positioned 1 inch in front of the dosing tube. Exposures of (R)-3-methylcyclohexanone were done using background (non-line-of-sight) exposures. The quadrupole mass spectrometer used for desorption measurements is enclosed in a stainless steel tube, terminating in a circular aperture approximately 0.75 cm in diameter. Desorption measurements were made with the sample positioned 3-4 mm from the aperture. The aperture is smaller than the diameter of the crystal and meant to minimize the measurement of species desorbing from surfaces other than the crystal surface facing the mass spectrometer. Desorption measurements were performed by heating the sample at a constant rate while the mass spectrometer monitored the species desorbing from the surface.

Results

Low Energy Electron Diffraction (LEED)

LEED patterns for stepped and kinked surfaces arise from diffraction off the terraces and spot splitting due the steps in the surface.[5] The terrace widths of stepped surfaces can be calculated from the magnitude of the spot splitting.[5,6] The angle between the primary spots from the terraces and the split spots from the steps provides information about the orientation of the kinks with respect to the lattice vectors of the terraces in real space. The real space structures and the LEED patterns for the $Cu(643)^R$ and $Cu(643)^S$ surfaces are shown in Figure 1. Both LEED patterns were taken with a primary electron beam energy of 183.0 eV while the crystal temperature was 85 K.

The lattice parameter of a bulk face-centered cubic Cu crystal is 3.61 Å.[7] The terrace width was calculated to be 11.4 Å, following the kinematic method of Henzler.[6] This corresponds to three atom wide terraces. A vector connecting the split spots on the $(643)^R$ diffraction pattern are at an angle of approximately -23° degrees with respect to the vertical direction and a vector connecting the split spots on the $(643)^S$ diffraction pattern is at an angle of approximately +23° with respect to the vertical direction. The direction of the spot splitting is reversed between the $(643)^R$ and $(643)^S$ surfaces and indicates the "handed" relationship between the two surfaces. The handedness of the real space

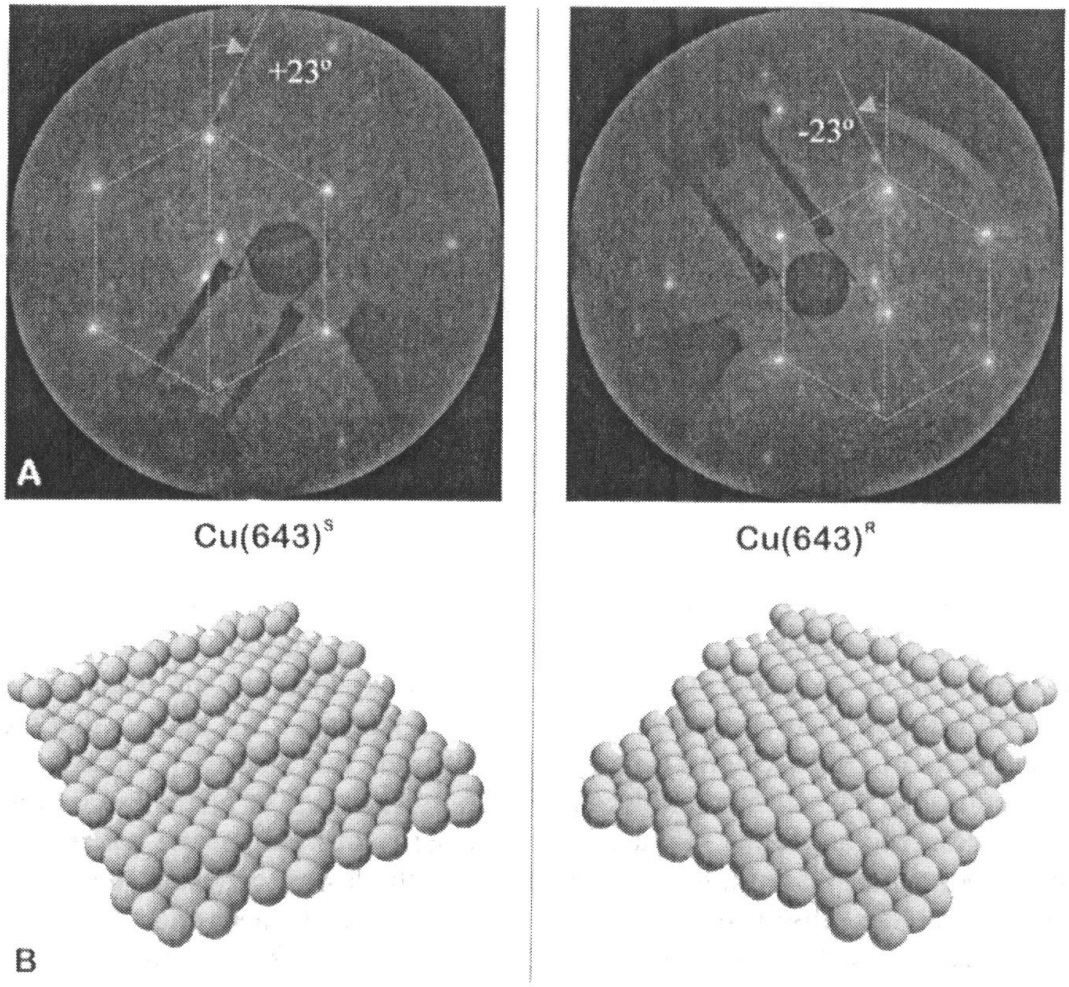

Figure 1. (A) Photographs of the LEED patterns from the Cu(643)^S and Cu(643)^R surfaces. The sample temperature is 85 K and the electron beam energy is 183.0 eV. (B) Three dimensional ball models of the Cu(643)^S and Cu(643)^R surfaces. The handedness of the real space structures is evident in the handedness of the diffraction patterns.

structure is evident in the handedness of the diffraction patterns. The LEED patterns observed for the $Cu(643)^R$ and $Cu(643)^S$ surfaces are in good agreement with previously published LEED patterns for Ag(643) and Pt(643) surfaces.[1,4]

Temperature-Programmed Desorption (TPD)

1-Chloro-2-methylbutane

TPD spectra were acquired for (S)-1-chloro-2-methylbutane and a racemic mixture of (R/S)-1-chloro-2-methylbutane on $Cu(643)^R$. If enantiospecific desorption occurs, the TPD spectra for these two samples should be different. Specifically, differences should exist between peak desorption temperatures for (S)-1-chloro-2-methylbutane and (R/S)-1-chloro-2-methylbutane desorbing from the same chiral surface. Peak temperature differences as small as 1 K are detectable with the equipment currently in use.

TPD spectra were acquired for (S)-1-chloro-2-methylbutane on $Cu(643)^R$ by direct exposure to the clean surface. After exposure to the chiral molecule, the surface was heated at a constant rate of 2 K/sec while positioned in front of the mass spectrometer detector. The fragments at m/q=29 and 41 were monitored. The background mass spectrum analysis of (S)-1-chloro-2-methylbutane showed that the signal from the fragment at m/q=29 was 5% more intense than the signal at m/q=41. However, when measuring the species desorbing from the Cu(643) surface during TPD experiments, the fragment at m/q=41 was 10% more intense than the signal at m/q=29. We believe that the desorption of (S)-1-chloro-2-methylbutane from the Cu(643) surface is molecular, but a small fraction decomposed on the surface to give alkyl groups which desorbed as olefins. Figure 2 shows a series of TPD spectra taken after increasing exposures from 0.05 L to 0.40 L. At the lowest exposure (0.05L), a single peak was observed at 260.5 K, corresponding to desorption from the monolayer. Due to some noise in the TPD spectra, peak temperatures were determined by Gaussian curve fitting on an interval ±10 K from the temperature at which the maximum desorption rate was recorded. Following an exposure of 0.20 L, the monolayer is saturated and the peak temperature has shifted slightly to 252.2 K. At an exposure of 0.40 L, a zero order peak corresponding to multilayer desorption is visible at 143.0 K. TPD spectra for (R/S)-1-chloro-2-methylbutane on $Cu(643)^R$ were obtained under the same conditions. Figure 3 shows the monolayer desorption peak temperatures for (S)-1-chloro-2-methylbutane and (R/S)-1-chloro-2-methylbutane on $Cu(643)^R$ as a function of increasing coverage. Coverages are given in terms of monolayers (ML), where 1 ML is the exposure at which the multilayer desorption peak becomes visible in the TPD spectrum. Coverages were determined by scaling the area under each TPD curve by the area under the saturated monolayer peak. As Figure 3 illustrates, the peak desorption temperatures for the pure enantiomer and the racemic mixture of 1-chloro-2-

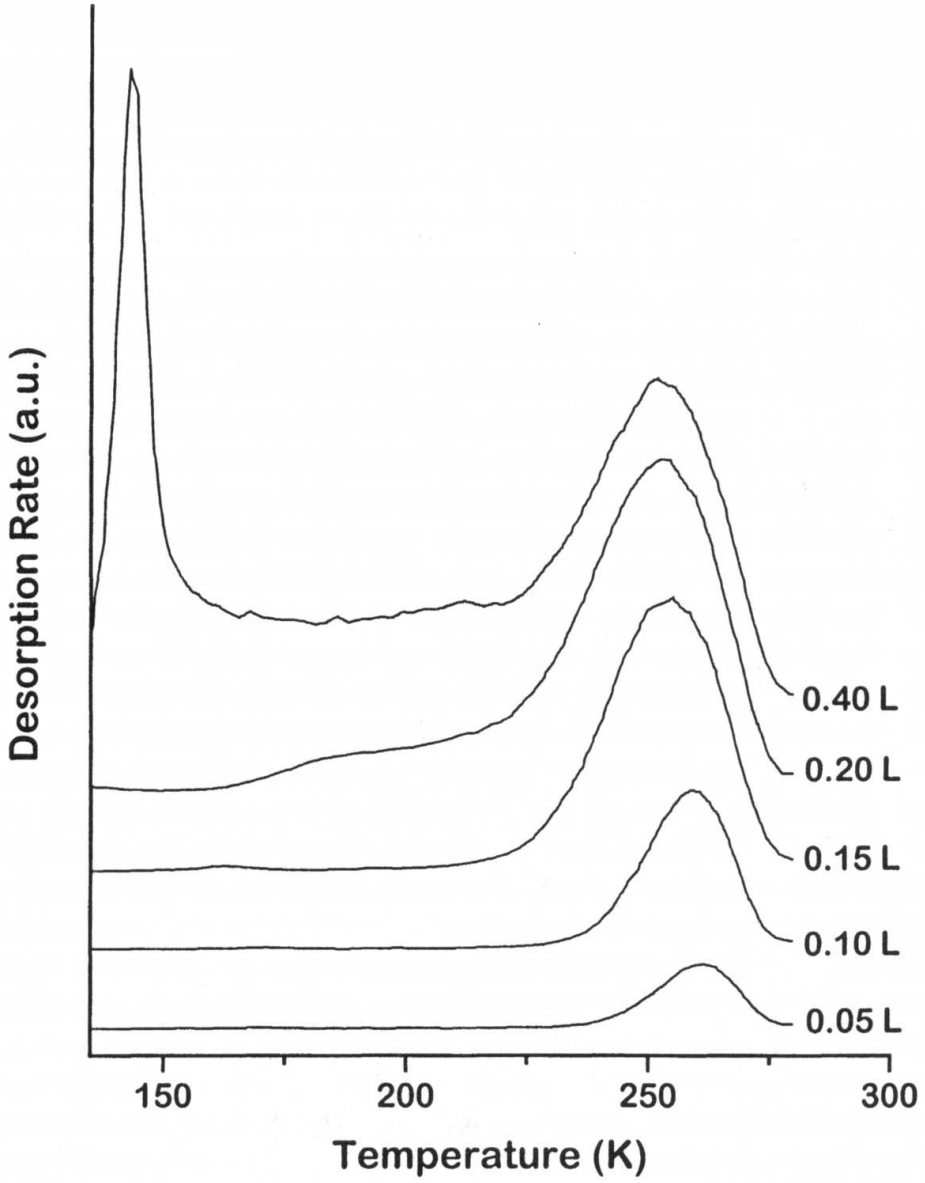

Figure 2. A series of TPD Spectra taken following increasing exposures of (S)-1-chloro-2-methylbutane to the Cu(643)^R surface, while monitoring the fragment at m/q = 41. The high temperature peak (~250 K) corresponds to monolayer desorption of molecules adsorbed directly to the Cu(643)^R surface, while the low temperature peak (143 K) corresponds to multilayer desorption. Curves are offset for clarity.

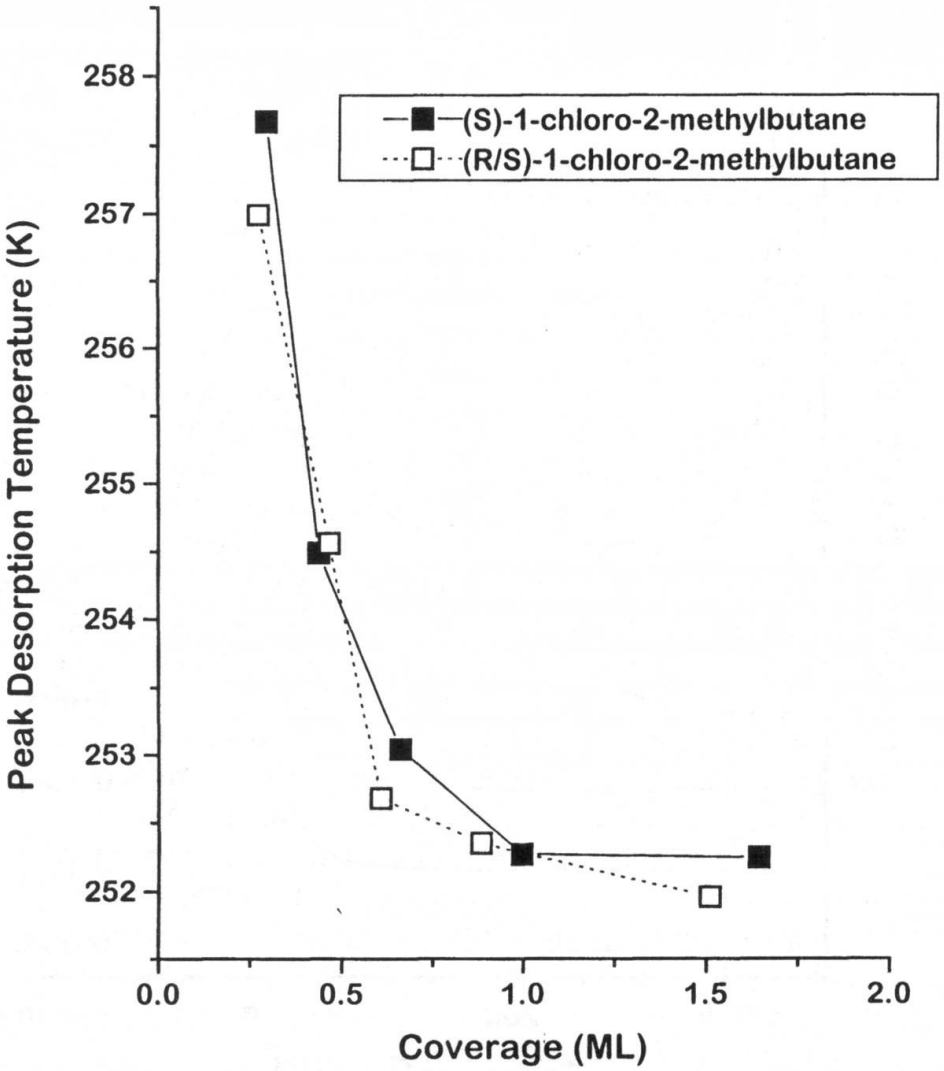

Figure 3. Peak desorption temperatures for (S)-1-chloro-2-methylbutane and (R/S)-1-chloro-2-methylbutane on Cu(643)^R plotted as a function of surface coverage. No enantiospecific differences are visible between the desorption characteristics of (S)-1-chloro-2-methylbutane and (R/S)-1-chloro-2-methylbutane on the Cu(643)^R surface.

methylbutane on the $Cu(643)^R$ surface are nearly identical. Thus, any enantiospecific effects are too small to measure for this particular system.

3-Methylcyclohexanone

TPD spectra were acquired for (R)-3-methylcyclohexanone ((R)-3MCHO) and a racemic mixture of (R/S)-3-methylcyclohexanone ((R/S)-3MCHO) on the $Cu(643)^R$ and $Cu(643)^S$ surfaces. These TPD experiments were conducted with background exposures to the clean Cu(643) surface at 90 K. After exposure to the chiral molecule, the surface was heated at a constant rate of 1 K/sec while positioned in front of the mass spectrometer. Figure 4 shows TPD spectra for (R)-3-MCHO on $Cu(643)^S$ following exposures from 0.05 L to 0.45 L. (R)-3-MCHO shows several peaks in its TPD spectrum. At the lowest exposure (0.05 L) two overlapping peaks are visible. Again the positions of the maxima have been determined by fitting a Gaussian function through the points lying ±10K from the maximum. A more intense peak is present at 386.4 K and a less intense peak is present at 349.1 K. The origin of the two peaks is not known at this time, however they must correspond to different adsorption states on the $Cu(643)^S$ surface. It is possible that one peak corresponds to desorption of molecules adsorbed in the kink sites of the surface and the other peak corresponds to molecules adsorbed to the flat (111) terraces of the surface. At the highest exposure (0.45 L), a zero-order desorption peak corresponding to multilayer desorption appears at 171.0 K. TPD spectra for (R)-3-MCHO on $Cu(643)^R$ and (R/S)-3-MCHO on $Cu(643)^R$ and $Cu(643)^S$ were also obtained and the results were qualitatively similar to the spectra in Figure 4. Initially several ionization fragments were monitored in the mass spectrometer in order to determine if 3-methylcyclohexanone was reacting on the surface. The relative intensities of the fragments monitored in the TPD experiments corresponded to the relative intensities of the fragments monitored during a background analysis of the vapor and there was not evidence of decomposition.

Careful examination of the TPD spectra described above reveals that the peak temperatures depend on the chirality of the adsorbed species and of the surface. Figure 5 shows the peak desorption temperatures for (R)-3-MCHO and (R/S)-3-MCHO on $Cu(643)^R$ and $Cu(643)^S$ as a function of surface coverage. Figure 5 only considers the highest temperature peak in the TPD spectra for 3-methylcyclohexanone on the Cu(643) surfaces. Surface coverage was determined by scaling the area under each TPD curve by the area under the two highest temperature peaks, once saturated. Figure 5 shows that the racemic mixture of (R/S)-3-MCHO has peak desorption temperatures on the $Cu(643)^R$ and $Cu(643)^S$ surfaces that are within 1.0 K for similar exposures. As the racemic mixture contains an equal amount of both enantiomers of 3-methylcyclohexanone, enantiospecific behavior is not expected and is not

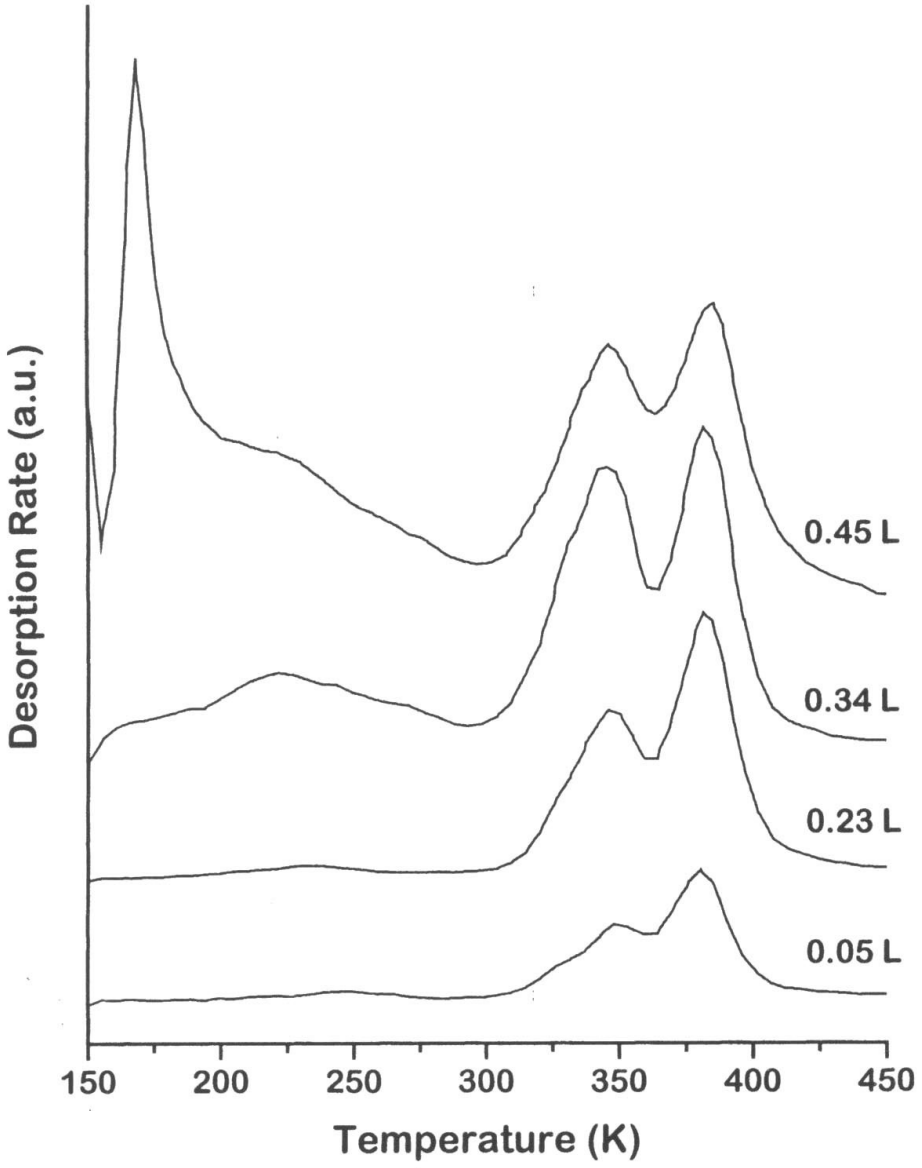

Figure 4. A series of TPD Spectra taken following increasing exposures of (R)-3-methylcyclohexanone to the Cu(643)^S surface, while monitoring the fragment at m/q = 39. The two highest temperature peaks (~350K, ~385 K) correspond to different adsorption states for (R)-3-MCHO on the Cu(643)S surface, while the low temperature peak (171 K) corresponds to multilayer desorption. Curves are offset for clarity.

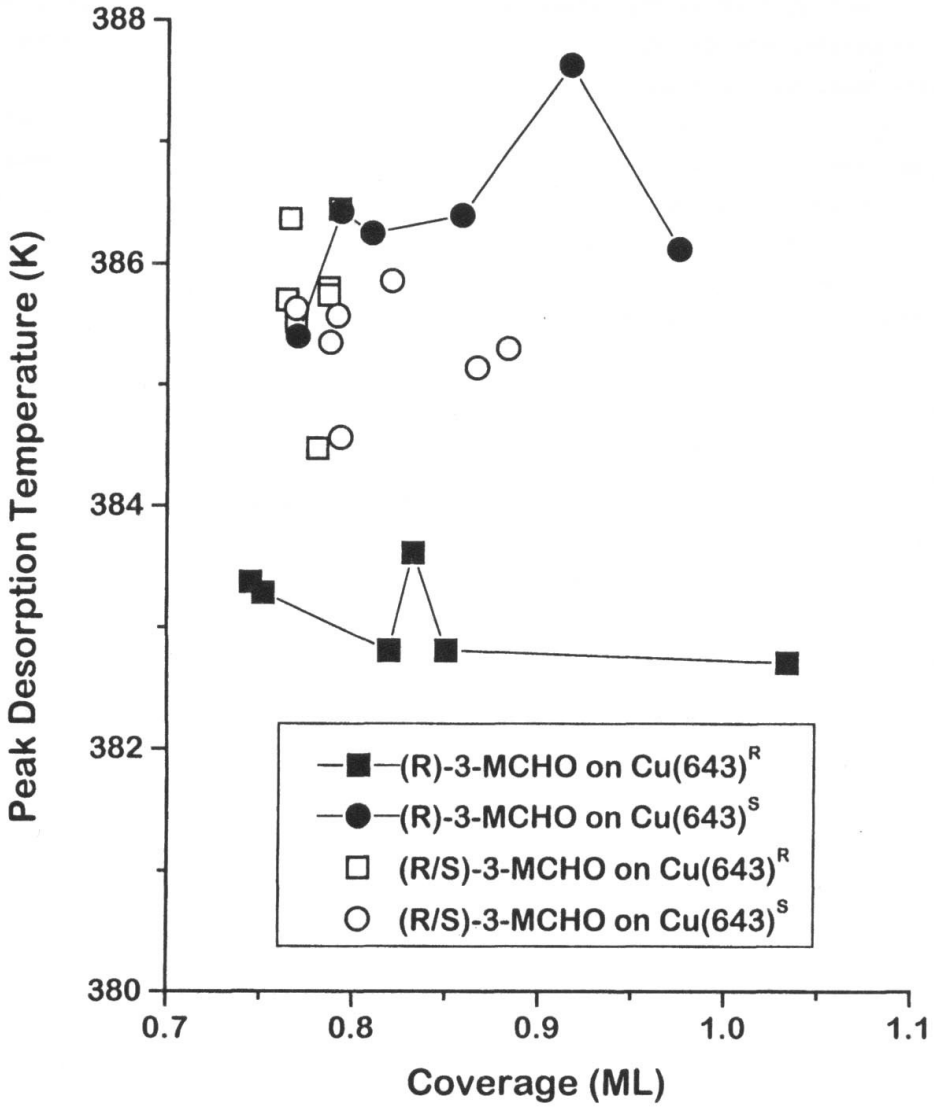

Figure 5. Peak desorption temperatures for (R)-3-methylcyclohexanone and (R/S)-3-methylcyclohexanone on Cu(643)^R and Cu(643)^S as a function of surface coverage. The racemic mixture of (R/S)-3-MCHO has similar peak desorption temperatures on both Cu(643)^R and Cu(643)^S surfaces. Enantiospecific effects are evident as the peak desorption temperatures for the pure enantiomer of (R)-3-MCHO differ by ~3.5 K between the Cu(643)^R and Cu(643)^S surfaces. This corresponds to a difference in desorption energies of 0.2 kcal/mol for (R)-3-MCHO on the Cu(643)^R and Cu(643)^S surfaces.

observed. (R)-3-MCHO on the $Cu(643)^S$ surface has peak desorption temperatures that are approximately 1-2 K higher than the racemic (R/S)-3-MCHO on the same surface. In contrast, (R)-3-MCHO on the $Cu(643)^R$ surface has peak desorption temperatures that are 2-3 K lower than the racemic (R/S)-3-MCHO on the same surface. These results clearly reveal enantiospecific adsorption is occurring on the chiral Cu(643) surface. Table I shows the average peak desorption temperature (T_p) and the average desorption energy (E_{des}) for each of the systems described above. Average peak desorption temperatures were calculated by averaging all data points collected for each adsorbate/surface combination. Average desorption energies were calculated using the standard relation for first-order desorption kinetics ($T_p^2=(\beta E_{des}/R\nu_1)\exp(E_{des}/RT_p)$) with an assumed preexponential factor (ν_1) of 10^{13} s^{-1}. In this equation, T_p is the peak desorption temperature, β is the heating rate, and E_{des} is the desorption energy for an unactivated process. The difference in E_{des} between (R)-3-MCHO on the $Cu(643)^R$ and $Cu(643)^S$ surfaces is ~0.2 kcal/mol.

Table I

System	*Avg. T_p (K)*	*Avg. E_{des} (kcal/mol)*
(R/S)-3-MCHO on $Cu(643)^R$	385.72 ± 0.65	24.83 ± 0.04
(R/S)-3-MCHO on $Cu(643)^S$	385.34 ± 0.42	24.80 ± 0.03
(R)-3-MCHO on $Cu(643)^R$	383.10 ± 0.37	24.65 ± 0.02
(R)-3-MCHO on $Cu(643)^S$	386.37 ± 0.72	24.87 ± 0.05

Note: Error ranges given are ± 1 standard deviation from the calculated values.

Theoretical Results

To complement the experiments described above, we have performed a series of theoretical calculations examining the adsorption of chiral hydrocarbons on chiral Pt surfaces. These calculations extend our previous studies of these systems.[2,8] For brevity, we will only describe our calculations involving the Pt(643) surface. We have also simulated a range of other Pt surfaces and will report on these results elsewhere.[9] In our simulations, the Pt surface is held rigid in the relaxed structure predicted for Pt(643) using density functional theory in the local density approximation.[10] Hydrocarbon molecules are modeled using the united atom approximation with bond bending and torsion angles described using the parameterization of Grest *et al.*[11] A bond

stretching potential was fitted to spectroscopic data[8] and an anti-inversion potential[11] was included to avoid the unphysical interconversion of enantiomers that is possible with united atom models. We have confirmed that gas phase simulations of these molecules reveal the correct distribution of molecular conformations for the molecules discussed below.[12] The interaction potential between hydrocarbon molecules and the Pt surface was defined using a potential fitted by Stinnett *et al.* to molecular beam scattering data.[13] The possible configurations for isolated adsorbates were explored using hybrid Monte Carlo trajectories including $> 10^7$ sample configurations per adsorbate. Energy minimization was applied to these sample configurations to determine adsorption geometries that are local minima on the potential energy surface.

The methods outlined above were applied to four chiral hydrocarbons, namely, trans-1,2-dimethyl-cyclo-X, where X = propane, butane, pentane, and hexane. We will abbreviate these molecules by DMCPr, DMCB, DMCPe, and DMCH. For each molecule, the stable adsorption geometries for both enantiomers were computed on the Pt(643) surface. Although every molecule exhibits multiple adsorption geometries, here we will only discuss the most stable (i.e., global energy minimum). For DMCPr and DMCB, the R enantiomer is more stable than the S enantiomer by 0.27 and 0.31 kcal/mol, respectively. The R enantiomer is also more stable for DMCPe, but only by 0.054 kcal/mol. By contrast, the S enantiomer's energy minimum lies 0.11 kcal/mol below the R enantiomer for DMCH. Qualitatively, the same trends are observed when thermal averages over all accessible minimum energy states are considered.[9] Three of the four molecules simulated yield enantiospecific differences in energy similar to those reported above for (R)-3-MCHO on Cu(643) and for glucose on Pt(643).[4] However, for one molecule, the enantiospecific energy difference is small enough that it would not be detected in our TPD experiments, even though this quantity is nonzero. This type of situation may account for our experimental results with (S)-1-chloro-2-methylbutane.

Conclusions

Several demonstrations of the enantiospecific properties of chiral single-crystalline surfaces have been observed. Through the observations of LEED patterns that are nonsuperimposable mirror images of each other, the $Cu(643)^R$ and $Cu(643)^S$ are shown to be enantiomers of each other. Similar LEED results have been observed elsewhere for Ag(643) and Pt(643) surfaces.[1,3,4] Theoretical calculations have shown that certain hydrocarbons on chiral Pt(643) surfaces exhibit enantiospecific adsorption characteristics. Experimental results from TPD show that the desorption energies of (R)-3-methylcyclohexanone on $Cu(643)^R$ and $Cu(643)^S$ differ by approximately 0.2 kcal/mol. Other work has

shown enantiospecific adsorption of glucose enantiomers on chiral Pt electrodes through electro-oxidation experiments.[3,4]

Acknowledgement.

This work was supported by NSF grant CTS-9813937. DSS and TDP acknowledge access to the CLAN cluster managed by the Pittsburgh Supercomputer Center.

References

1. McFadden, C.F.; Cremer, P.S.; Gellman, A.J. *Langmuir*. **1996**, 12, 2483-2484.
2. Sholl, D.S. *Langmuir*. **1998**, 14, 862-867.
3. Ahmadi, A.; Attard, G.; Feliu, J.; Rodes, A. *Langmuir*. **1999**, 15, 2420-2424.
4. Attard, G.A.; Ahmadi, A.; Feliu, J.; Rodes, A.; Herrero, E.; Blais, S.; Jerkiewicz, G. *Journal of Physical Chemistry B*. **1999**, 103, 1381-1385.
5. Ertl, G.; Küppers, J. *Low Energy electron and Surface Chemistry*, 2nd ed.; VCH: Weinheim, 1985; pp 246-2488.
6. Henzler, M. *Surface Science*. **1970**, 19, 159-171.
7. Kittel, C. *Introduction to Solid State Physics*, 7th ed.; John Wiley and Sons: NY, 1996.
8. Power, T.D.; Sholl, D.S. *Journal of Vacuum Science Technology A*. **1999**, 17, 1700-1704.
9. Power, T.D.; Sholl, D.S. submitted to *Topics in Catalysis*.
10. Feibelman, P. J. *personal communication*.
11. Mondello, M.; Grest, G.S. *J. Chem. Phys.* **1995**, 103, 7156.
12. Eliel, E.L.; Wilen, S.H. *Stereochemistry of Organic Compounds*; John Wiley and Sons: New York, 1994.
13. Stinnett, J.A.; Madix, R.J.; Tully, J.C. *J. Chem. Phys.* **1996**, 104, 3134.